



Design method for calculating settlement of stiffened deep mixed column-supported embankment over soft clay

Zhen Zhang¹ · Feng-Rui Rao¹ · Guan-Bao Ye¹

Received: 25 November 2017 / Accepted: 30 January 2019 / Published online: 9 February 2019
© Springer-Verlag GmbH Germany, part of Springer Nature 2019

Abstract

As a composite column, stiffened deep mixed (SDM) column is formed by inserting a precast concrete core pile into the center of a deep mixed (DM) column. The SDM columns have been successfully used to support highway and railway embankments and buildings over soft soil. However, there has been still a lack of feasible method to calculate the settlement of SDM column-reinforced soft soil under an embankment load. This paper developed a theoretical solution to calculate the settlement of SDM column-supported embankment over soft soil. Based on the unit cell concept, the total settlement of the SDM column-reinforced soft soil consisted of three components, i.e., the compression of soil within the length of stiffened core pile, the compression of soil from the core pile base to the SDM column base, and the compression of soil below the SDM column base. The upward and downward penetrations of stiffened core pile were considered in the analysis. The analytical solution was verified by a comparison with the results computed by three-dimensional finite element analyses. A parametric study based on the derived solution was conducted to investigate the influence factors of modulus, length and diameter of DM column, length and diameter of core pile, and interface friction angle between DM column and core pile on the settlement of SDM column-reinforced soil, and some recommendations were proposed for its application in practice. The design charts for settlement calculation were developed for the ease of use in design. The design method was applied to two case histories of SDM column-supported embankments, and good agreements were found between the predicted settlements and the field measurements.

Keywords Embankment · Settlement · Soft clay · Stiffened deep mixed column · Theoretical analysis

List of symbols

l_1, l_2, l_3	Original thicknesses of Region I, Region II, and Region III, respectively	D_e, B	Equivalent diameter of influence zone and column spacing, respectively
l'_1, l'_2, l'_3	Thicknesses of Region I, Region II, and Region III when the unit cell is subjected to a surface pressure, respectively	$S_{\text{total}}, S_{\text{I}}, S_{\text{II}}, S_{\text{III}}$	Total settlement and the compression of Region I, Region II, and Region III, respectively
l_0	Depth of equal settlement plane	$\delta_{\text{up}}, \delta_{\text{down}}, \delta_{\text{core}}$	Upward penetration and downward penetration of the core pile; the compression of the core pile, respectively
D, d	Diameter of DM column and core pile, respectively	S_{su}, δ_1	Compression of the surrounding soil and the compression of core pile above the neutral point, respectively
		S_{sd}, δ_2	Compression of the surrounding soil and the compression of core pile below the neutral point, respectively
		$\Delta F, \Delta z$	Change in axial force at two adjacent depths and the distance between the two adjacent depths, respectively
		τ_0	Negative friction at the elevation of core pile head

✉ Guan-Bao Ye
guanbaoye@gmail.com

Zhen Zhang
dyzhangzhen@gmail.com

Feng-Rui Rao
704819763@qq.com

¹ Department of Geotechnical Engineering, Tongji University, 1239 Siping Road, Shanghai 200092, China

$\tau(z)$	Skin friction stress at a depth of z
K	In situ coefficient of lateral earth pressure
φ, φ_i	Friction angle of DM column and the interface friction angle between the core pile and the DM column, respectively
P, σ_p, σ_s	Applied pressure on the whole area of the unit cell, the average vertical stress on the top of core pile and the equivalent surrounding soil, respectively
m, α	Replacement ratio of SDM column and core pile area ratio in cross section of SDM column, respectively
λ, γ	Ratio used in derivation
E_1^{eq}, E_{sI}	Equivalent constrained modulus of surrounding soil and DM column, the constrained modulus of subsoil in Region I, respectively
$\sigma_{sz}, \sigma_{pz}, \sigma_{sl_1}, \sigma_{pl_1}$	Vertical stress at certain depth
A_c, A_p	Areas of influence zone and core pile, respectively
u_p	Perimeter of core pile
p_c, p_s	Upward penetration when a unit force is exerted on the top of core pile and downward penetration when a unit force exerted on the bottom of core pile, respectively
l_{GC}, E_{GC}	Thickness of gravel cushion and the constrained modulus of cushion, respectively
μ_0	Poisson's ratio of DM column
E	Constrained modulus of soil layer
μ	Poisson's ratio of soil layer
k	Coefficient of permeability
σ_1, σ_2	Vertical stress on the bottom of Region I and vertical stress on the bottom of Region II, respectively
η	Coefficient of average superimposed stress
n	Stress concentration ratio
a, b, c, u, v, s	Variations used in design method

1 Introduction

Columns are commonly used to improve soft soils by increasing the bearing capacity, reducing total and differential settlements, and enhancing stability. Recently,

columns have been increasingly used to support embankments over soft soils, especially when the requirements for settlement control and/or construction time are strict. Different types of columns have been used in practice, such as stone columns, deep mixed (DM) columns, jet grouted columns, vibro-concrete columns (VCCs), cement-fly ash-gravel (CFG) columns, T-shaped DM columns and rammed aggregate piers [6, 25–29, 32, 35, 39, 45]. Furthermore, composite columns have been increasingly used in practice, since they take advantages of positive effects of the individual components (e.g., concrete piles for strength and stiffness, and DM columns for increasing soil strength).

As a composite column, stiffened deep mixed (SDM) column is formed by inserting a precast concrete core pile into the center of a DM column immediately after the construction of the DM column (see Fig. 1) [40]. Concrete core pile is installed to increase the strength and stiffness of the column and reduce the ground settlement, meanwhile, DM column is used to increase the skin friction of the core pile shaft and reinforce the surrounding soil. Moreover, the bearing capacity provided by SDM columns was similar to the cast-in-place piles with the same diameter and length, while the SDM column can save nearly 30% cost [30].

In the past decade, the behavior of SDM column-reinforced soft soil was investigated mostly by means of experimental and numerical studies [31, 33, 40]. Tanchaisawat et al. [31] experimentally found that the shear strength of the interface between concrete core pile and DM column was increased linearly with the unconfined compressive strength of soil–cement. Voottipruex et al. [33] indicated that the settlement on SDM column was 40% less than that of DM columns due to its higher stiffness. Ye et al. [40] found that the critical height of soil arching in the SDM column-supported embankment had a good consistency with the clear spacing between the concrete core piles based on the three-dimensional finite element analysis.

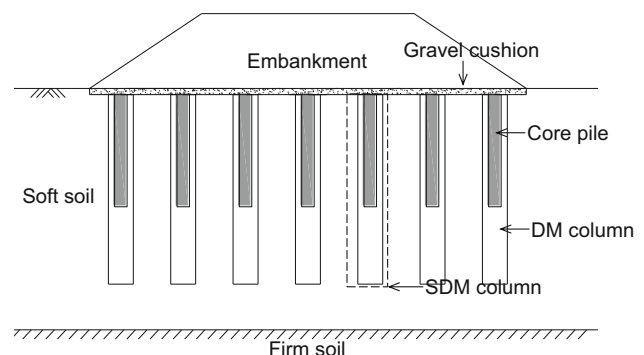


Fig. 1 SDM column-supported embankment over soft soil

The system of SDM column-reinforced soft soil is composed of three materials (i.e., core pile, DM column, and soft soil) and two interfaces (i.e., interface between core pile and DM column and interface between DM column and surrounding soil). Due to the complicity of this system, there have been only a few publications dealing with the theoretical analysis of SDM column-reinforced soft soil [20, 30, 37]. Wu et al. [37] proposed a method to calculate the bearing capacity of SDM column by assuming that the failure in the surrounding soil triggered the failure of SDM column. Jamsawang et al. [20] and Raongjant and Jing [30] indicated that the lateral bearing capacity of SDM column was 11–15 times and 3–4 times greater than that of DM column under static and cyclic loading, respectively.

At present, there is no applicable design method for calculating the settlement of SDM column-reinforced soft soil. Many studies have been conducted focusing on the settlement calculation of other type of column-reinforced soft clay. Han [17] established a method for calculating the settlement of stone column-reinforced foundation. Zhang et al. [41] developed an analytical solution for the settlement of a composite foundation reinforced with stone columns considering that the modulus of column had reduction effects on column settlements and bulging. Abdelkrim and Buhan [1] presented an elastoplastic homogenization method applied to a soil reinforced by regularly distributed columns. Castro and Sagaseta [7] presented an approximate solution to calculate the settlement of rigid footing resting on a stone column-reinforced soft soil by converting the column group to an axisymmetric problem with an equivalent single column with the same cross-sectional area.

Horikoshi and Randolph [18] proposed a simplified design method to calculate the settlement of piled rafts. Han and Wayne [16] demonstrated that the method proposed by Horikoshi and Randolph [18] for piled rafts can also be used to calculate the settlement of DM column-reinforced soft soil. Yao et al. [38] conducted a 1-g physical model test for soft ground with deep mixed columns considering the effect of column length, area replacement ratio and surcharge load on foundation settlement. Chai et al. [8] proposed a method to calculate the settlement of DM column-reinforced foundations underlain by a soft soil, in which the penetration of the columns was considered by treating the lower portion of the reinforced zone as an “unreinforced” layer. Therefore, it is necessary to develop a calculation method for the settlement of SDM column-reinforced soft soil.

In this paper, a theoretical analysis was conducted to derive a solution of the settlement of stiffened deep mixed column-supported embankment over soft clay. The unit cell concept is adopted to establish the calculation model and the subsoil is assumed to settle under one-dimensional

condition. The settlement of subsoil consists of three components, i.e., the compression of the soil within length of stiffened core piles, the compression of the soil from core pile base to SDM column base and the compression of the soil below SDM column base. The upward and downward penetrations of concrete core pile were considered in the analysis. To validate the developed analytical method, three-dimensional (3-D) finite element models with different configurations of SDM columns were created and the comparison between the analytical predictions and the numerical results were discussed. A parametric study based on the derived solution was performed to investigate the influence factors of DM column modulus, length of core pile and DM column, diameter of DM column and core pile, and interaction coefficient on the settlement characteristic of SDM column-reinforced soil, and some recommendations are summarized for its application. Finally, the design charts were drawn for ease of application in design. Two case histories of SDM column-supported embankment over soft soil were introduced and the design method was applied to predict the ground final settlements.

2 Derivation of settlement of the foundation

2.1 Calculation model

The unit cell concept is adopted to establish the calculation model. The unit cell analysis is valid only when it is applied at the embankment centerline where the lateral displacements are zero, but it cannot successfully predict the settlement on other places under embankment where the lateral displacements took place. However, in design of an embankment over soft soil, engineers pay more attention on the settlement of ground surface at the centerline of embankment, since it is the maximum value along the embankment width.

Figure 2 shows the unit cell of SDM column-reinforced soil in the analysis, in which the unit cell is divided into three regions in the cross section: Region I (the region from ground surface to core pile base), Region II (the region from core pile base to DM column base), and Region III (the region of soft soil below DM column base). In Fig. 2, l_1 , l_2 and l_3 are the original thicknesses of Region I, Region II, and Region III, respectively; l'_1 , l'_2 and l'_3 are the thicknesses of Region I, Region II, and Region III, respectively, when the unit cell is subjected to a surface pressure P ; D and d are the diameters of DM column and core pile; and D_e is the equivalent diameter of influence zone, in which $D_e = 1.05B$ for columns in a triangular pattern; $D_e = 1.13B$ for columns in a square pattern; and B is the column spacing.

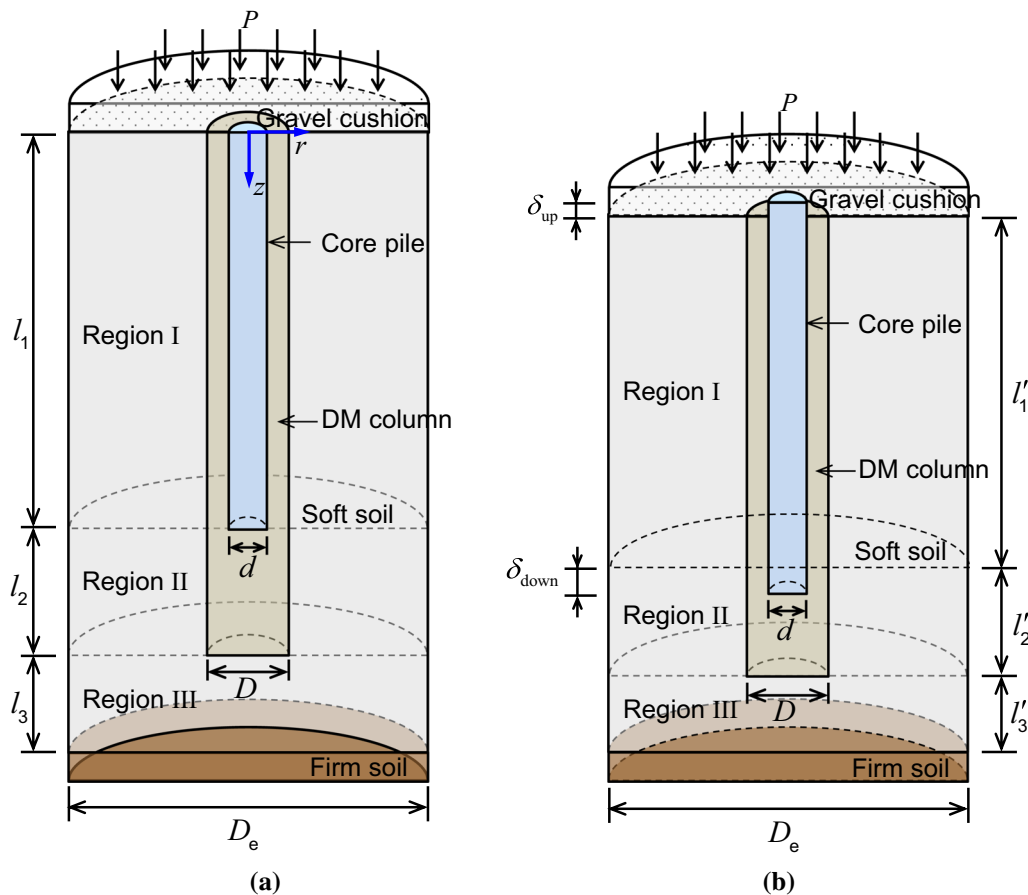


Fig. 2 Unit cell of SDM column-reinforced soil: **a** before settlement, **b** after settlement

The main assumptions made in the analysis are summarized as: (a) the concrete core pile, the DM column and the subsoil behave as isotropic linear-elastic materials; (b) the radial deformation is ignored and only vertical strain is considered; (c) the surrounding soil and the DM column in Region I and Region II are treated as a composite soil with equivalent constrained modulus.

Based on the division of the regions in the unit cell of the analytical model, the total settlement of SDM column-reinforced subsoil can be expressed as:

$$S_{\text{total}} = S_{\text{I}} + S_{\text{II}} + S_{\text{III}}, \quad (1)$$

in which S_{total} is the total settlement; S_{I} is the compression of Region I; S_{II} is the compression of Region II; and S_{III} is the compression of Region III. Referring to Fig. 2, $S_{\text{I}} = l_1 - l'_1$, $S_{\text{II}} = l_2 - l'_2$, and $S_{\text{III}} = l_3 - l'_3$. The following sections discuss the derivations of settlement calculation for each Region.

2.2 Compression of soil in Region I

In the system of SDM column-supported embankment, gravel cushion is commonly placed on the top of pile head

to adjust stress transfer between pile and soil. Due to the great difference in stiffness between pile and soil, more vertical stress is concentrated onto the core pile when it is subjected to the embankment load. As a result, the core pile would penetrate upward into the cushion layer and downward into the DM column under the embankment load. This phenomenon is called stress concentration effect and has been observed in the previous studies on pile-reinforced soil with a gravel cushion on the top surface [44]. On the other hand, the differential settlement between the pile and the soil results in the shear stress developing in the fill, which would increase the stress carried by the pile and reduce the stress carried by the soil. This stress transfer phenomenon is referred to as soil arching effect. To simplify the analysis, this study did not consider the soil arching effect (i.e., the shear stress developed in the gravel fill is neglected) but considered the stress concentration effect. In the unit cell model, the modulus of gravel cushion is considered but the embankment fill is equivalent to a uniform pressure applied on the cushion surface. This model is conservative as the stress imposed on the soil is overestimated. The derivation process is introduced in this section.

Considering the core pile penetration effect (see Fig. 2), one can obtain:

$$S_I = l_1 - l'_1 = \delta_{up} + \delta_{down} + \delta_{core}, \tag{2}$$

in which δ_{up} is the upward penetration of the core pile; δ_{down} is the downward penetration of the core pile; and δ_{core} is the compression of the core pile. Since the surrounding soil in the shallow portion settles more than the core pile under the embankment load, negative frictional force occurs on the core pile shaft. Considering the existence of neutral point due the negative friction on the shaft of core pile, Eq. (2) is rewritten as:

$$S_I = S_{su} + S_{sd} = (\delta_{up} + \delta_1) + (\delta_{down} + \delta_2), \tag{3a}$$

$$S_{su} = \delta_{up} + \delta_1, \tag{3b}$$

$$S_{sd} = \delta_{down} + \delta_2, \tag{3c}$$

in which S_{su} and δ_1 are the compressions of the surrounding soil and the core pile above the neutral point, respectively; and S_{sd} and δ_2 are the compressions of the surrounding soil and the core pile below the neutral point, respectively.

Figure 3a shows the distribution of the skin frictional stresses along the core pile under different embankment height based on the field measurements by Wang et al. [34]. The skin frictional stress of core pile was calculated by the equation, $\tau_z = \Delta F / (u_p \Delta z)$, in which ΔF is the change in axial force at two adjacent depths (kN); Δz is the distance between the two adjacent depths (m); and, u_p is

the perimeter of core pile. The absolute values of the skin frictional stress (i.e., negative and positive skin friction) along the core pile increased with the increase in embankment height while the depth of neutral point was almost kept constant during the whole loading procedure. It should be realized that the location of neutral point dynamically changes with time and fill load. In this field test, the fill height was only 3.5 m. The small embankment loading results in a relative stable location of neutral point in the whole filling process. This phenomenon has also been found by Kong [24]. For a better presentation, the skin frictional stress along the core pile shaft was normalized to a ratio of the skin frictional stress at a given depth to the maximum positive skin friction. It is worth noticing from Fig. 3b that the skin frictional stress along the core pile had a consistent normalization with depth and the distribution of the skin frictional stress along the core pile could be approximated as a linear distribution. Therefore, the skin frictional stress along the core pile is assumed to be a linear distribution (see Fig. 4) in this analysis.

The basic Coulomb friction model was used to calculate the negative skin friction between the core pile and the DM column. The interface friction angle is considered, but the cohesion of DM column/core pile interface is ignored. The interfacial cohesion would decrease under certain conditions under the long-term condition. For example, when the interface is fully soaked, the interfacial cohesion would decrease [10, 14]. When a relative large displacement

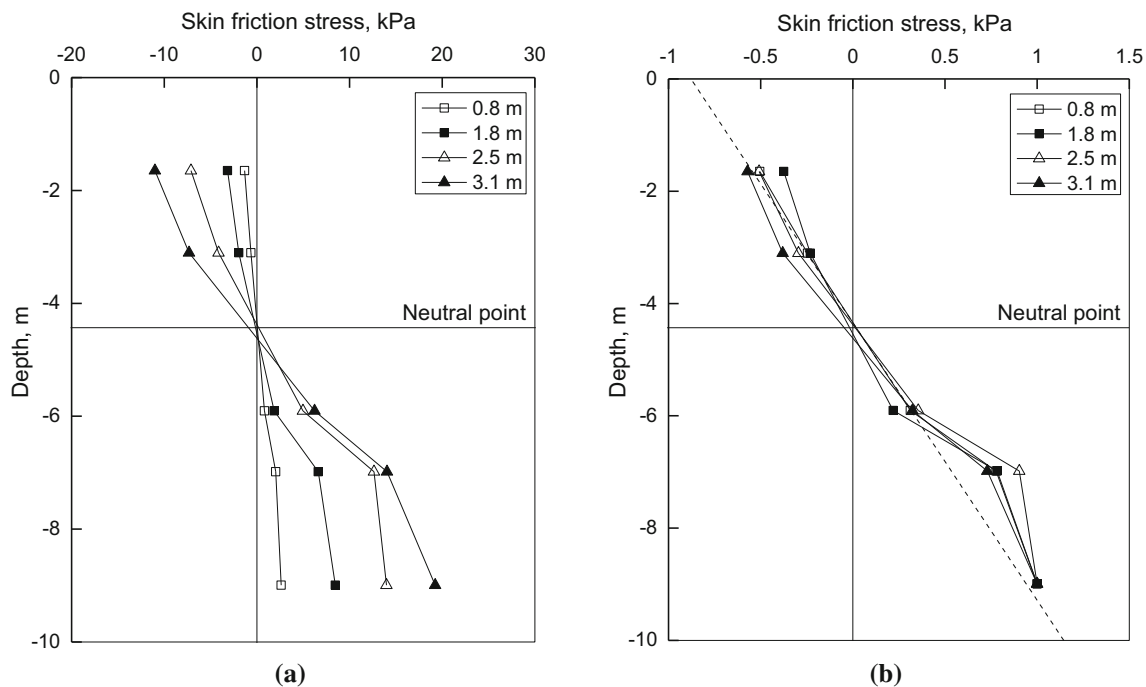


Fig. 3 Consideration of skin friction distribution along concrete core pile

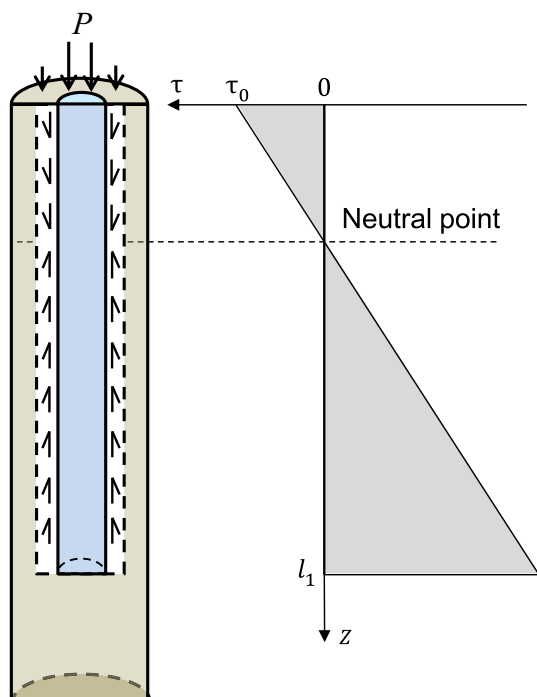


Fig. 4 Simplification of skin friction distribution along concrete core pile

between core pile and DM column develops, the interfacial cohesion would also decrease due to the full slip [5, 21]. From a practical point of view, it is conservative to ignore the cohesion of DM column/core pile interface for a long-term performance. The maximum negative skin friction is expressed as follows [4]:

$$\tau_0 = K\sigma_s \tan \varphi_i \tag{4}$$

in which τ_0 is the negative friction at the core pile head; φ_i is the interface friction angle between the core pile and the DM column; σ_s is the vertical stress on the top of surrounding soil; K is the in situ lateral earth pressure coefficient. The in situ lateral earth pressure coefficient is complicated and is dependent on soil type, pile material, and method of pile installation [36]. For a convenient use in design, K value is recommended in a range of lateral earth pressure coefficient at rest (i.e., $K = 1 - \sin\varphi$, where φ is the effective friction angle of deep mixed soil) to passive lateral earth pressure coefficient [i.e., $K = \tan^2(45^\circ + \varphi/2)$]. If there is no test result available to determine φ , 30° is recommended to use in design [2, 13, 43]. Therefore, K value is in a range of 0.5–3 when $\varphi = 30^\circ$. For a displacement core pile, as driving process causes the soil to be displaced radially, a relatively large K value is recommended, and for a non-displacement and/or partial displacement core pile, as the soil is removed, a relatively small K value is recommended. However, a selection of specific value still relies on engineers’

experience and judgment. Three case histories were selected to verify the applicability of the proposed method to determine K value. Wu et al. [37] conducted a field investigation in which the core pile was driven directly into a DM column. Based on the field results, the back-calculated K was 1.9 by taking $\varphi = 30^\circ$ and $\varphi_i = 18^\circ$, which approaches the passive lateral earth pressure coefficient [i.e., $K = \tan^2(45^\circ + \varphi/2) = 3$]. Ding et al. [11] reported a field test in which the core pile was installed by a partially bored method. Based on the field results, the back-calculated K was 0.6, close to the lateral earth pressure coefficient at rest (i.e., $K = 1 - \sin\varphi = 0.5$). Voottipruex et al. [33] presented a field pullout test of core pile which was driven directly into a DM column, and the back-calculated K was 1.3 which is also within the proposed range.

To demonstrate the feasibility of Eq. (4) for estimating the maximum negative friction on the core pile shaft, a comparison between the field test results by Wang et al. [34] and the calculated negative friction by Eq. (4) was conducted. The measured skin frictional stresses of core pile were obtained based on the measured vertical stress of the pile head and the measured point close to the pile head using the equation of $\tau_z = \Delta F / (u_p \Delta z)$. The meanings of notations have been explained previously. In the analysis, the interface friction angle of the DM column and the core pile was taken as 18° [31]. Considering the core pile was directly pushed into the ground, resulting in increasing the lateral earth pressure in the field, the K value was larger than the coefficient of earth pressure at rest. The K value was assumed to be passive lateral earth pressure coefficient in the analysis. It can be seen from Fig. 5 that the calculated skin friction agreed well with the measured results under the different fill load.

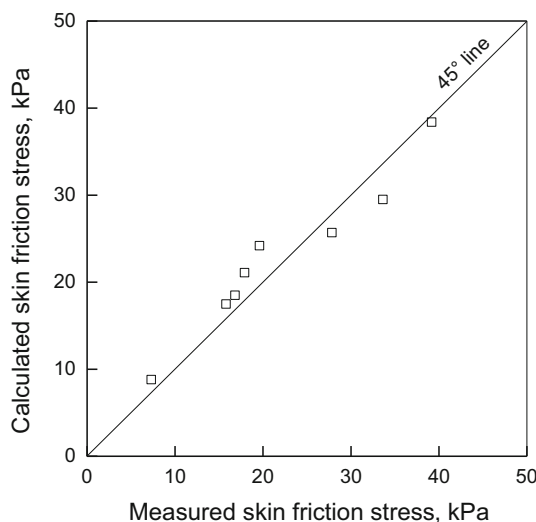


Fig. 5 Comparison of skin friction between measured and calculated results

According to the triangular pattern assumption of the skin friction stress along the core pile, the concrete core skin friction is written as:

$$\tau(z) = -\tau_0(1 - z/l_0), \tag{5}$$

in which $\tau(z)$ is the skin friction stress at a depth of z (i.e., a negative value means the negative friction, vice versa); l_0 is the depth of equal settlement plane, and z is the depth from ground surface.

Based on the force equilibrium in vertical direction, both the SDM column and the equivalent surrounding soil carry the applied loads, and thus,

$$P = m\alpha\sigma_p + (1 - m\alpha)\sigma_s. \tag{6a}$$

Setting the stress concentration ratio $n = \sigma_p/\sigma_s$, one can obtain

$$\sigma_p = \frac{nP}{(n - 1)\alpha m + 1}, \tag{6b}$$

$$\sigma_s = \frac{P}{(n - 1)\alpha m + 1}, \tag{6c}$$

in which P is the applied pressure on the whole area of the unit cell; m is the replacement ratio of SDM column, i.e., $m = D^2/D_e^2$; α is the core pile area ratio in cross section of SDM column, i.e., $\alpha = d^2/D^2$; σ_p and σ_s are the average vertical stress on the top of core pile and the equivalent surrounding soil, respectively.

The equivalent constrained modulus of surrounding soil and DM column in Region I (E_1^{eq}) is determined based on the area-weighted average of DM column socket and surrounding soil:

$$E_1^{eq} = m(1 - \alpha)E_{DM} + (1 - m)E_{sI}, \tag{7}$$

in which E_1^{eq} is the equivalent constrained modulus of surrounding soil and DM column; E_{DM} is the constrained modulus of DM column; E_{sI} is the constrained modulus of subsoil in Region I.

Figure 6 shows a slice element of the unit cell with a thickness of dz at a depth z . Based on the equilibrium of force in the slice element in a vertical direction, one can obtain:

$$\sigma_{sz}(A_e - A_p) - (\sigma_{sz} + d\sigma_{sz})(A_e - A_p) - \tau_z u_p dz = 0, \tag{8}$$

in which σ_{sz} is the average vertical stress on surrounding soil and DM column at depth z ; A_e and A_p are the areas of influence zone and core pile, respectively; and u_p is the perimeter of core pile.

Setting $\lambda = u_p/(A_e - A_p)$, Eq. (8) is rearranged as:

$$d\sigma_{sz}/dz + \lambda\tau_z = 0. \tag{9}$$

Using the boundary condition, $\sigma_{sz} = \sigma_s$, at $z = 0$, Eq. (9) is solved as:

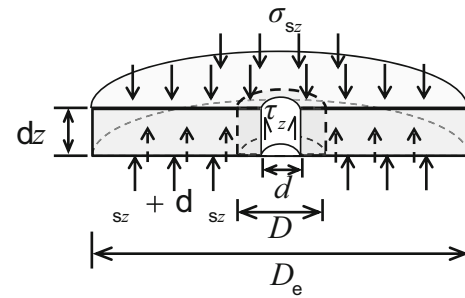


Fig. 6 Force analysis on calculation unit

$$\sigma_{sz} = (\lambda\tau_0 z^2)/(2l_0) - \lambda\tau_0 z + \sigma_s. \tag{10}$$

Thus, the compression of subsoil in Region I can be derived as:

$$S_{su} = \int_0^{l_0} (\sigma_{sz}/E_1^{eq}) dz = \frac{1}{E_1^{eq}} \left(\sigma_s l_0 - \frac{\lambda\tau_0}{3} l_0^2 \right), \tag{11a}$$

$$S_{sd} = \int_{l_0}^{l_1} (\sigma_{sz}/E_1^{eq}) dz = \frac{1}{E_1^{eq}} \left(\frac{\lambda\tau_0}{6l_0} l_1^3 - \frac{\lambda\tau_0}{2} l_1^2 + \sigma_s l_1 - \sigma_s l_0 + \frac{\lambda\tau_0}{3} l_0^2 \right). \tag{11b}$$

All the above notations have been explained previously.

At depth z , based on the vertical force equilibrium on core pile shaft, the vertical stress in core pile can be expressed as:

$$\sigma_{pz} = \sigma_p + A_p^{-1} \int_0^z \tau_z u_p dz = \sigma_p + \gamma(\tau_0 z - \tau_0 z^2/(2l_0)), \tag{12}$$

in which $\gamma = u_p/A_p$. Similarly, the compression of core pile in Region I can be derived as:

$$\delta_1 = \int_0^{l_0} (\sigma_{pz}/E_p) dz = \frac{1}{E_p} (\sigma_p l_0 + \gamma\tau_0 l_0^2/3), \tag{13a}$$

$$\delta_2 = \int_{l_0}^{l_1} (\sigma_{pz}/E_p) dz = \frac{1}{E_p} \left(-\frac{\gamma\tau_0}{6l_0} l_1^3 + \frac{\gamma\tau_0}{2} l_1^2 + \sigma_p l_1 - \sigma_p l_0 - \frac{\gamma\tau_0}{3} l_0^2 \right). \tag{13b}$$

The upward penetration of core pile can be determined as:

$$\delta_{up} = p_c(\sigma_p - \sigma_s), \tag{14a}$$

where p_c is the upward penetration when an unit force is exerted on the top of core pile, and it can be obtained as:

$$p_c = l_{GC}/E_{GC}, \tag{14b}$$

in which l_{GC} is the thickness of gravel cushion, and E_{GC} is the constrained modulus of cushion.

The downward penetration of core pile can be determined as:

$$\delta_{\text{down}} = p_s(\sigma_{pl_1} - \sigma_{sl_1}), \tag{15a}$$

in which σ_{pl_1} is the vertical stress at the bottom of core pile; σ_{sl_1} is the vertical stress at the bottom of subsoil; and p_s is the downward penetration when an unit force exerted on the bottom of core pile which can be calculated based on the method proposed by Chen [9],

$$p_s = (1 - \mu_0^2)\omega\sqrt{A_p}/E_0 \tag{15b}$$

$$E_0 = (1 - 2\mu_0^2/(1 - \mu_0))E_{II}^{\text{eq}} \tag{15c}$$

in which μ_0 is the Poisson’s ratio of DM column; ω is a parameter decided by the shape of loading plane; and E_{II}^{eq} is the equivalent constrained modulus of soil in Region II.

Thus, by combining Eqs. (11a), (13a), (14a), and (3b), one can obtain:

$$((\sigma_s l_0 - \lambda\tau_0 l_0^2/3)/E_I^{\text{eq}} = p_c(\sigma_p - \sigma_s) + (\sigma_p l_0 + \gamma\tau_0 l_0^2/3)/E_p \tag{16}$$

Similarly, combining Eq. (11b), Eq. (13b), Eq. (15a), and Eq. (3c) results in

$$\begin{aligned} & \frac{1}{E_I^{\text{eq}}} \left(\frac{\lambda\tau_0}{6l_0} l_1^3 - \frac{\lambda\tau_0}{2} l_1^2 + \sigma_s l_1 - \sigma_s l_0 + \frac{\lambda\tau_0}{3} l_0^2 \right) \\ &= \frac{1}{E_p} \left(-\frac{\gamma\tau_0}{6l_0} l_1^3 + \frac{\gamma\tau_0}{2} l_1^2 + \sigma_p l_1 - \sigma_p l_0 - \frac{\gamma\tau_0}{3} l_0^2 \right) \\ &+ p_s \left[\sigma_p - \sigma_s + (\gamma + \lambda)\tau_0 l_1 - \frac{(\gamma + \lambda)\tau_0 l_1^2}{2l_0} \right]. \end{aligned} \tag{17}$$

Substituting Eq. (4) into Eqs. (16) and (17), the stress concentration ratio can be expressed as:

$$n = \frac{\sigma_p}{\sigma_s} = \frac{\theta_1}{\theta_2} = \frac{\theta_3}{\theta_4}, \tag{18}$$

in which $\theta_1 = \frac{l_0}{E_I^{\text{eq}}} + p_c - \frac{\lambda K \tan \varphi_i}{3E_I^{\text{eq}}} l_0^2 - \frac{\gamma K \tan \varphi_i}{3E_p} l_0^2$; $\theta_2 = p_c + \frac{l_0}{E_p}$; $\theta_4 = p_s + \frac{(l_1 - l_0)}{E_p}$

$$\begin{aligned} \theta_3 = & \frac{1}{E_I^{\text{eq}}} \left(\frac{\lambda K l_1^3 \tan \varphi_i}{6l_0} - \frac{\lambda K l_1^2 \tan \varphi_i}{2} + l_1 - l_0 + \frac{\lambda K l_0^2 \tan \varphi_i}{3} \right) \\ & - \frac{1}{E_p} \left(-\frac{\gamma K l_1^3 \tan \varphi_i}{6l_0} + \frac{\gamma K l_1^2 \tan \varphi_i}{2} - \frac{\gamma K l_0^2 \tan \varphi_i}{3} \right) \\ & - p_s \left(-1 + (\gamma + \lambda) K l_1 \tan \varphi_i - \frac{(\gamma + \lambda) K l_1^2 \tan \varphi_i}{2l_0} \right). \end{aligned}$$

In Eq. (18), only l_0 is the unknown variation. By solving Eq. (18), l_0 and n can be obtained. Then σ_p and σ_s can also be solved by Eqs. (6b) and (6c). One can obtain S_{su} , S_{sd} , δ_1 , δ_2 from Eqs. (11a), (11b) and Eqs. (13a), and (13b), respectively. The settlement in Region I can be calculated as:

$$S_I = S_{su} + S_{sd} = (\lambda\tau_0 l_1^3 / (6l_0) - \lambda\tau_0 l_1^2 / 2 + \sigma_s l_1) / E_I^{\text{eq}}. \tag{19}$$

2.3 Compression of soil in Region II

The unconfined compressive strength of DM column is typically within a range of 0.4–1.5 MPa for the soft clays in practice [12]. The elastic modulus of DM columns could be estimated based on the typical relationship of $E = 100q_u$ [12, 19]. Thus, the elastic modulus of DM columns may be within a range from 40 to 150 MPa. Due to the relative low modulus difference between the DM columns and the surrounding soil as compared with the difference between rigid columns and the surrounding soil, it is assumed that the DM column and the surrounding soil settles under an equal strain condition in the analysis of the compression of the soil in Region II. Zhang et al. [42] also made an equal strain assumption when deriving the consolidation solution of a composite foundation with short DM columns and long PVDs and a good agreement was obtained as compared with the field data. The equivalent modulus of the soil in Region II is determined based on the area-weighted average of the constrained modulus of the DM column and the surrounding soft soil:

$$E_{II}^{\text{eq}} = mE_{DM} + (1 - m)E_{sII}, \tag{20}$$

in which E_{II}^{eq} is the equivalent constrained modulus of the improvement area in Region II; and E_{sII} is the constrained modulus of soil.

The stress solution for a three-layer system proposed by Jones [22] was used to calculate the vertical stresses on the top and bottom of Region II. The solution to the compression of the soil in Region II can be given as:

$$S_{II} = [(\sigma_1 + \sigma_2)l_2] / (2E_{II}^{\text{eq}}), \tag{21}$$

in which σ_1 is the vertical stress on the bottom of Region I; and σ_2 is the vertical stress on the bottom of Region II.

2.4 Compression of soil in Region III

The compression of soil in Region III is computed using Mindlin’s solution:

$$S_{III} = \eta\sigma_2 l_3 / E_{III}, \tag{22}$$

in which η is the coefficient of average superimposed stress; and E_{III} is the constrained modulus of soil in Region III.

Based on the above derivations, the solutions to the compressions of the three regions are developed. Substituting the compressions of the three regions into Eq. (1), the total settlement of the soil reinforced by SDM column can be obtained.

3 Model validation and parametric study

3.1 Model validation

To validate the derived solution of the settlement of SDM column-reinforced soil, a three-dimensional (3-D) finite element analysis incorporated in the software ABAQUS was adopted. The results calculated by the proposed analytical method were compared with the results by the 3-D numerical analysis. Three typical conditions were considered in the numerical models: (a) the SDM column with equal length of DM column and core pile were seated on a firm soil (Model 1); (b) the SDM column with DM column longer than core pile were seated on a firm soil (Model 2); (c) there was a weak underlying stratum below the base of SDM column with long DM column and short core pile (Model 3).

Figure 7 shows the configuration of Model 3. The subsoil consisted of a 15-m-thick soft soil underlain by a 5-m-thick firm soil layer. The SDM column had DM column with a diameter of 500 mm and a length of 10 m and concrete core pile with a diameter of 250 mm and a length of 6 m. The columns were installed in a square pattern at a spacing of 1.8 m. A 0.3-m-thick gravel cushion and 4.0-m-thick embankment fill were placed on the top of SDM column-reinforced soft soil. The other two numerical models (i.e., Model 1 and Model 2) had a same geological condition but different SDM column configuration. Figure 8 shows the mesh of Model 1. The 3-D finite element mesh consisted of 5714 C3D8 (i.e., an eight-node brick, trilinear displacement) solid elements for the meshes of core pile and 13039 C3D8R solid elements (i.e., an eight-node brick, trilinear displacement, reduced integration) for the meshes of cushion, DM column, and subsoils. Table 1 shows the geometrical information of the three numerical models. In some cases, the pile is modeled using structural element (for example, beam element or pile element) for simplicity and improving computation efficiency. The beam element is unable to obtain the stress distribution throughout the cross section. In this study, as it needs to obtain the stresses distributed on the cross section of pile to calculate the stress concentration ratio, the solid element instead of the structural element is used to simulate the pile. Furthermore, as the deformation of pile itself is very small under the embankment, the pile is modeled as elastic material with Young's modulus and Poisson's ratio. The sand cushion, the DM column, and the subsoil were modeled as linearly elastic–perfectly plastic materials with Mohr–Coulomb failure criteria [15, 40]. In the elastic part, the elastic modulus of DM column was determined based on the typical relationship of $E = 100q_u$, and the Poisson's ratio was estimated based on the empirical values. As the

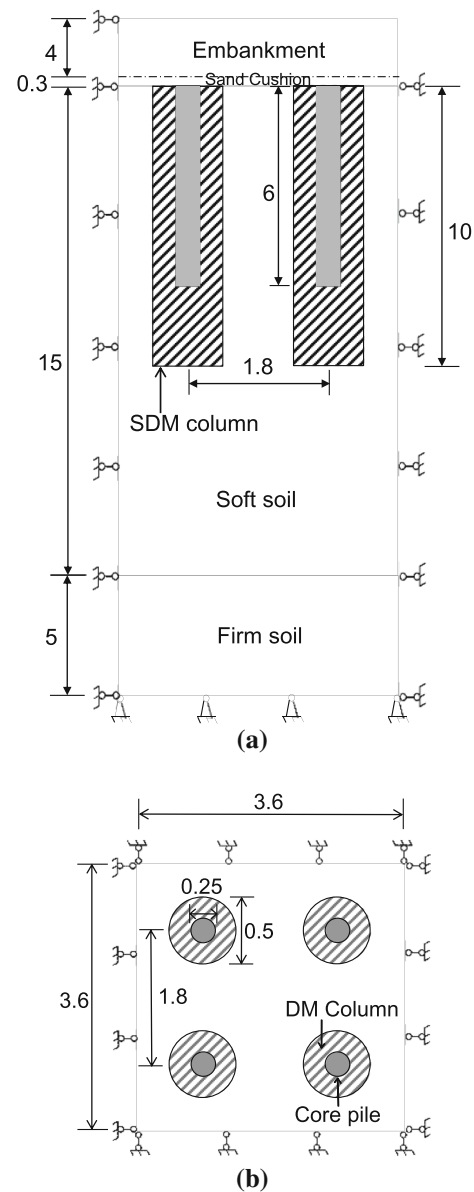


Fig. 7 Unit cell model for floating SDM pile supported embankment (not to scale; unit: m): **a** cross section, **b** plan view

unconfined compressive strength of 1 MPa is very common in practice, $E = 100$ MPa was used in the numerical analysis. In the plastic part, the friction angle was taken as 30° and the cohesion was estimated as half of the unconfined compressive strength (500 kPa) in this study. Various studies investigated the friction angle of soil–cement [2, 23, 43], and it is typically in a range of 20° – 35° . The parameters of concrete core pile can be obtained based on the criteria of concrete strength grades. The concretes with strength grades of C20–C35 (unconfined compression strengths from 20 to 35 MPa) are usually used to produce the core pile. Their corresponding elastic moduli are from 2.55 to 3.15 GPa, and the Poisson's ratio is typically from

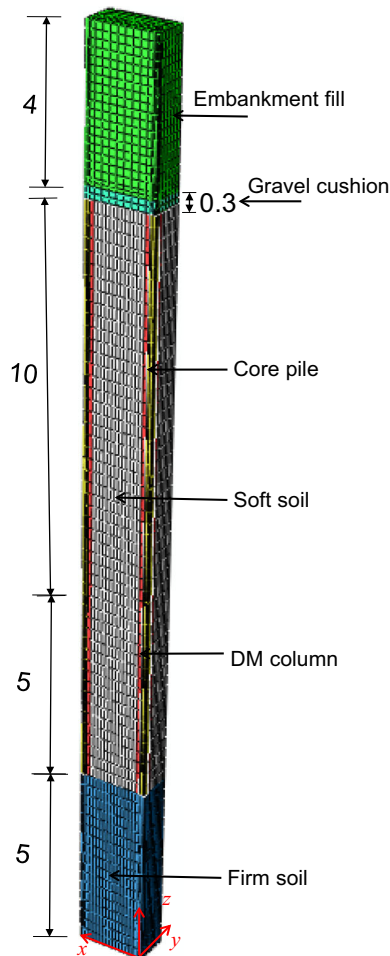


Fig. 8 3-D finite element mesh (unit: m)

Table 1 Geometrical information of numerical models

Model No.	Spacing (m)	DM column		Core pile	
		<i>D</i> (m)	<i>l</i> ₁ + <i>l</i> ₂ (m)	<i>d</i> (m)	<i>l</i> ₁ (m)
Model 1	1.8	0.5	15	0.25	15
Model 2	1.8	0.5	15	0.25	6
Model 3	1.8	0.5	10	0.25	6

0.1 to 0.22. In the numerical analysis, elastic modulus of 2.55 GPa and Poisson’s ratio of 0.15 were used. The interface contact was created between the concrete core pile and DM column with interfacial friction angle of 18° [31] and the shear stiffness coefficient $K_{ss} = 80$ MPa/m [31, 40]. Table 2 shows the material properties used in the numerical models. The four side boundaries of models were fixed in the lateral displacement but allowed to move freely in the vertical direction. The bottom boundary was fixed in all three directions (i.e., *x*, *y*, and *z* directions). After completion of the initial geostatic stress balance, the

Table 2 Main physico-mechanical parameters of materials in numerical analysis

Materials	<i>E</i> (MPa)	γ (kN/m ³)	μ	ϕ' (°)	<i>c'</i> (kPa)
Embankment Fill	30	18	0.30	32	0
Gravel cushion	30	18	0.30	35	0
Soft soil	5	18	0.42	15	8
Firm soil	100	20	0.30	32	300
DM column	100	20	0.33	30	500
Concrete core pile	25,500	25	0.15	N/A	N/A

E, elastic modulus, γ , unit weight, μ , Poisson’s ratio, ϕ' , effective friction angle, *c'*, effective cohesion

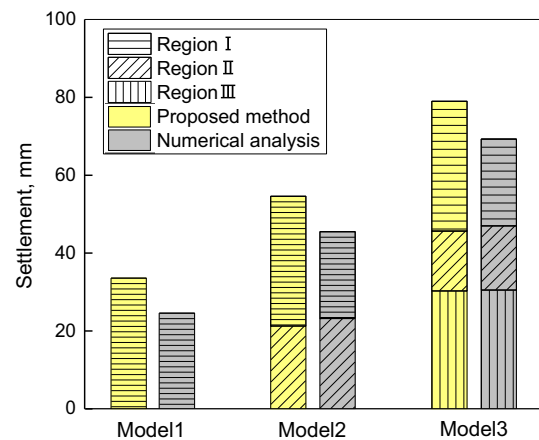


Fig. 9 Comparison of predictions by 3-D analysis and developed solution

sand cushion and embankment fill were placed on the base of SDM column-reinforced soil sequentially.

Figure 9 shows the settlements predicted by the numerical analysis and the developed solution. It can be seen that in the three models, the compressions in Region II and III by the numerical analysis and the developed solution agreed well with each other, while the compression in Region I by the developed solution was greater than that by the numerical analysis. In general, the proposed method properly revealed the deformation behavior of SDM column-supported embankment over soft soil.

3.2 Parametric study and discussion

To investigate the settlement characteristics of SDM column-reinforced soft soil, a parametric study was conducted in this section. In the baseline case, the soft soil consisted of a 15-m-thick soft soil. SDM columns were installed in a square pattern with a spacing of 1.8 m. The DM column had a diameter of 500 mm and a length of 10.0 m and the core concrete pile had a diameter of 250 mm and a length of 6.0 m. The interface friction angle was 18°. The gravel

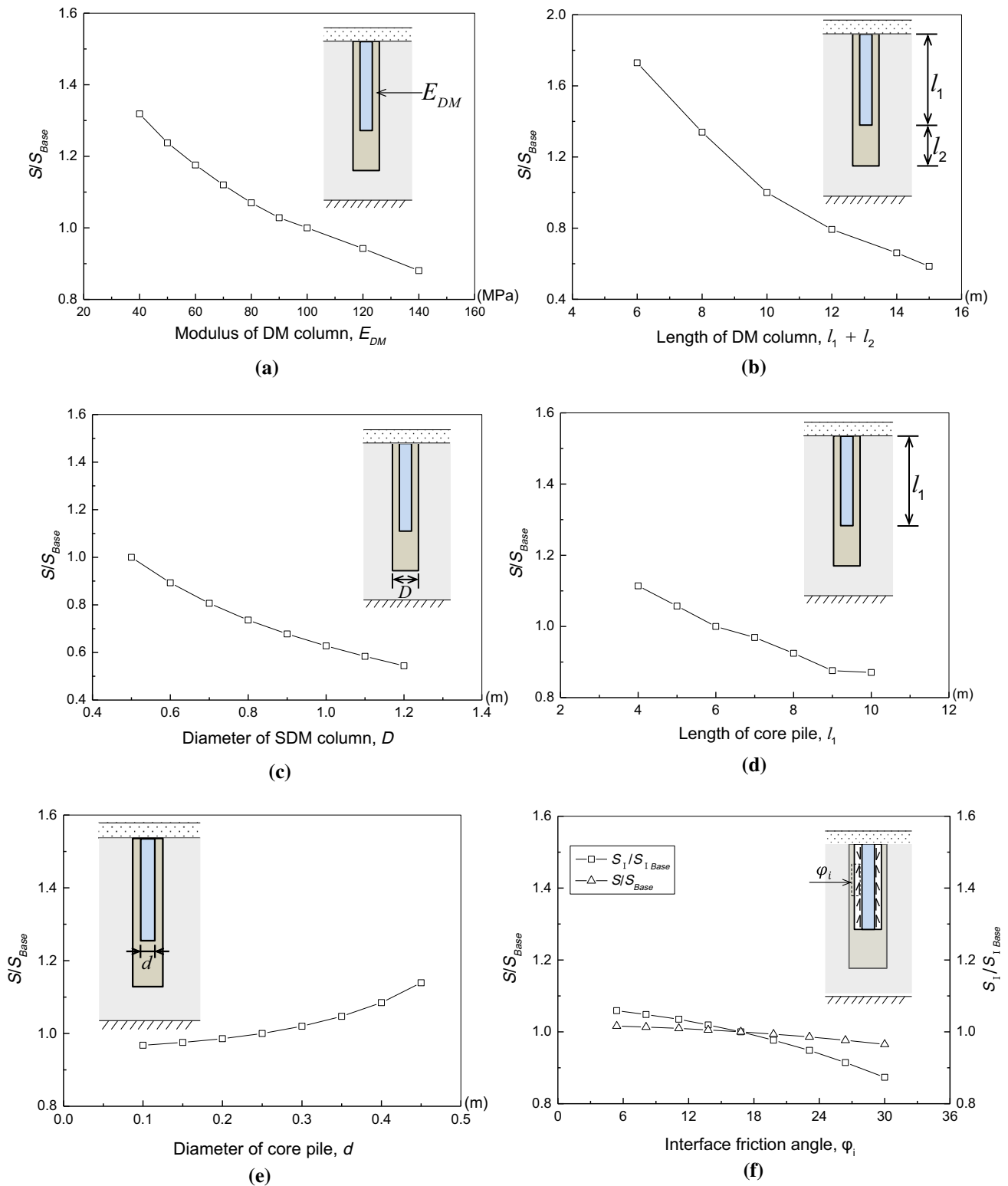


Fig. 10 Influence of different parameters on settlement: **a** modulus of DM column, **b** length of DM column, **c** diameter of SDM column, **d** length of core pile, **e** diameter of core pile, **f** interface friction angle

cushion had a thickness of 0.3 m and the embankment had a thickness of 4.0 m. The moduli of the soft soil, the DM column, the core pile and the gravel cushion were 5, 100,

and 28,000, 30 MPa, respectively. In the following analysis, the influence factors of DM column modulus, length of core pile and DM column, diameter of DM column and

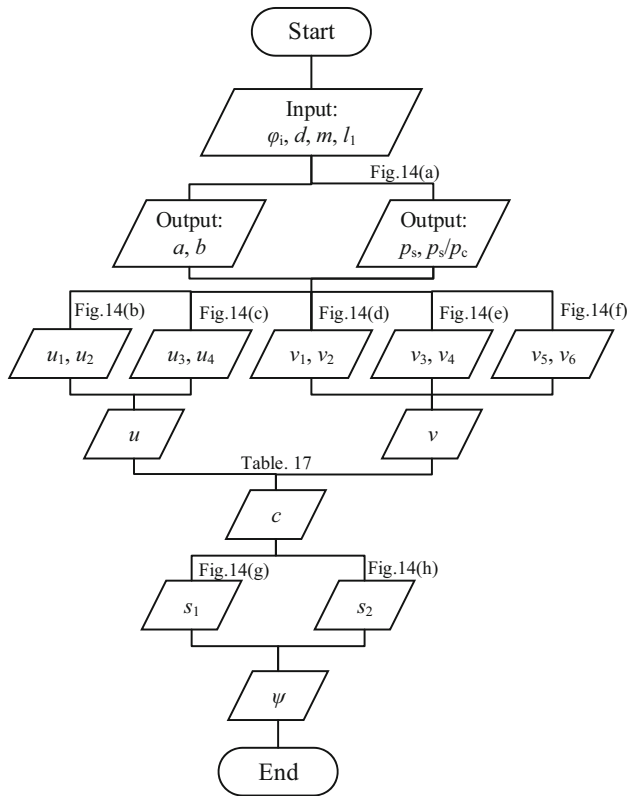


Fig. 11 Proceeding of design curves of Region I

core pile, and the interaction coefficient of the interface between DM column and core pile on the settlement characteristic of SDM column-reinforced soil were explored. In each case, only one influence factor was changed compared with the baseline case and a settlement ratio which is defined as a ratio of the settlement of the case with a changed parameter to that of the baseline case was introduced to investigate the role the influence factor played in the system. Based on the proposed method, the settlement of the baseline case was $S_0 = 131.5$ mm.

Figure 10 shows the change of settlement ratio with different influence factors. Figure 10a–c shows that the settlement of SDM-reinforced soft soil can be reduced by increasing the modulus, length, and diameter of DM column. Increasing the length of DM column had a significant influence on mitigating the settlement. Figure 10d, e shows that the settlement of SDM-reinforced soft soil was reduced by increasing the length of core pile, and the change in the diameter of core pile had less influence on the settlement than the change in the length of core pile. Voottipruex et al. [31] also indicated that the section area of concrete core pile had a slight effect on the settlement of SDCM column based on the numerical parametric analysis. However, when the length of core pile was greater than 9 m and the diameter of core pile changed from 0.15 to 0.25 m, which corresponded to the ratio of DM column length to core pile length of 0.9,

and the area ratio of core pile in the cross section of SDM from 10 to 25%, minor influences on mitigating settlement were obtained. Voottipruex et al. [33] found that the effective length ratio ranges from 0.57 to 0.85 in terms of the bearing capacity of SDM column. From a practical point of view, increasing the length of core pile is the preferred option on mitigating the settlement of soft soil when adopting the SDM column, and the optimal length and diameter of core pile should be considered in design.

Figure 10f shows that the settlement of ground was reduced slightly with the increase of interface friction angle ϕ_1 . It is because that the increase in the settlement due to the decrease in interface friction was small as compared with the total settlement. To clearly detect the effect of the interface, a ratio of the settlement in Region I between the case with a changed parameter to that of the baseline case was calculated alone, which is also included in Fig. 10f. It can be seen that the settlement ratio of Region I changes from 1.06 to 0.87 with an increase in interface friction angle from 6° to 30° . Therefore, the influence of interface friction angle is not as remarkable as the influence factors shown in the preceding Fig. 10a–e. This finding was similar to the numerical results by Voottipruex et al. [33].

4 Design method

Based on the above derivations, the settlements in Region II and Region III can be directly obtained based on the developed solutions, while the calculation of the settlement in Region I was complex. For a convenient application in design, this section developed a design procedure for the calculation of the settlement in Region I based on the derived solution. The proposed design method is applicable to the cases when the core pile length is smaller or equal to the length of DM column.

The settlement of Region I can be solved by Eq. (19). A 0.3-m-thick gravel cushion is typically used in practice, and thus the thickness of gravel cushion is kept constant as 0.3 m in the design method. Substituting Eqs. (4) and (6c) into Eq. (19), setting $a = \lambda k \tan \phi_i / 3$, $b = \gamma k \tan \phi_i / 3$, and ignoring the terms with E_p as they were small enough due to the large magnitude of E_p as the denominator, Eq. (19) is converted as follows:

$$S_I = P\psi = P \left(\frac{al_1^3 / (2l_0) - 1.5al_1^2 + l_1}{am(l_0 - al_0^2) / p_c + E_1^{eq}} \right), \tag{23a}$$

$$\delta l_0^3 + \zeta l_0^2 + \varepsilon l_0 + \xi = 0, \tag{23b}$$

in which $\delta = a(2 + 2p_s/p_c)$; $\zeta = -\delta/a$; $\varepsilon = 2l_1 - 3al_1^2 - 6p_s(a + b)E_1^{eq}$; $\xi = al_1^3 + 3p_s(a + b)l_1E_1^{eq}$. Setting $c = l_0/l_1$ and thus Eqs. (23a) and (23b) is calculated as:

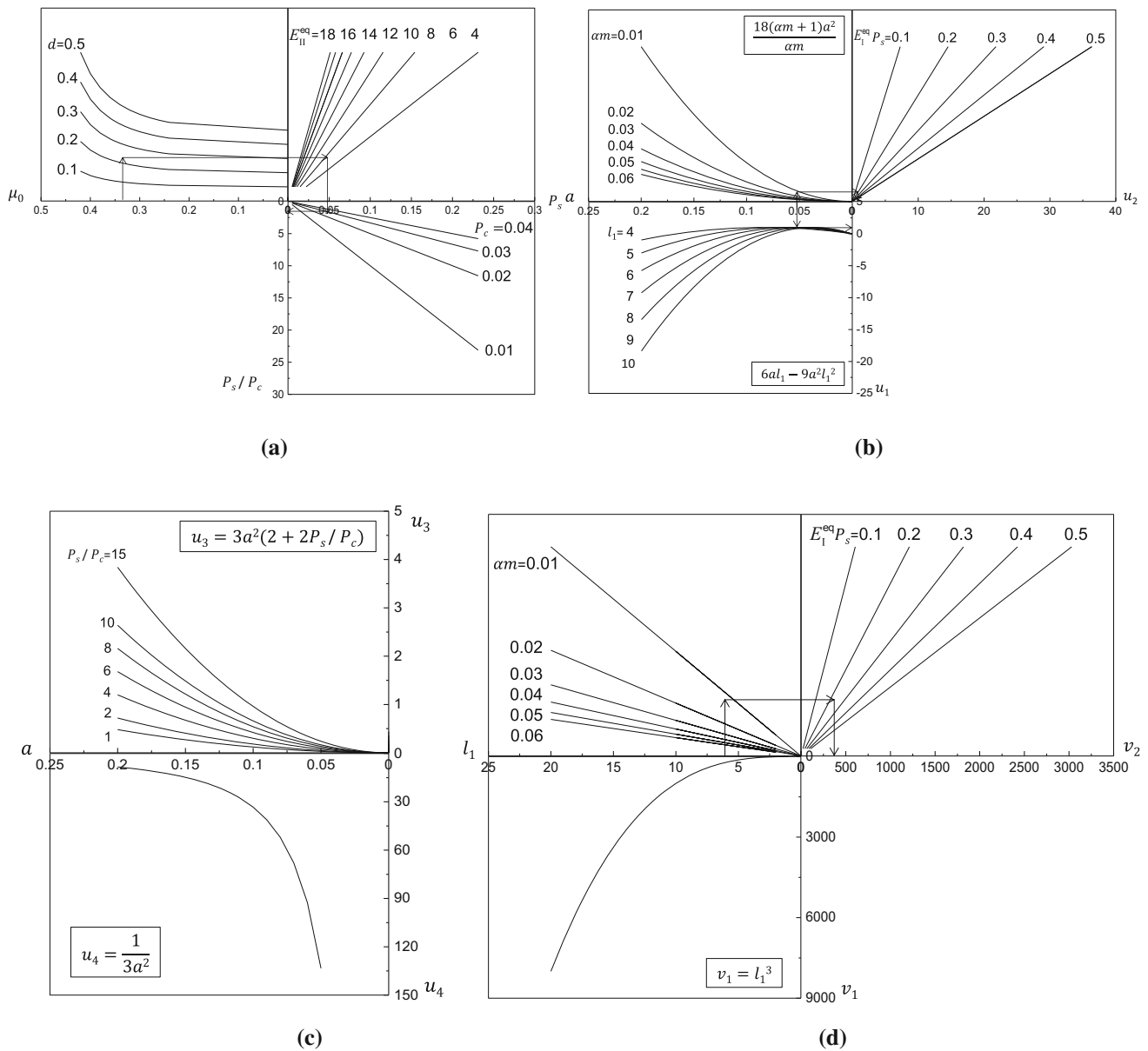


Fig. 12 Settlement design curves of Region I

$$S_I = P\psi = P \left(\frac{al_1^2/(2c) - 1.5al_1^2 + l_1}{\alpha m (cl_1 - ac^2l_1^2)/p_c + E_I^{eq}} \right), \tag{24a}$$

$$\delta l_1^3 c^3 + \zeta l_1^2 c^2 + \varepsilon l_1 c + \xi = 0. \tag{24b}$$

A design procedure is recommended herein to determine ψ , which is also summarized in the flow chart as shown in Fig. 11. The design charts corresponding to the flow chart are presented in Fig. 12. For the charts illustrated with a linear distribution, it is reasonable to extend the lines if the variable is not in the domain presented in the chart. The design procedure is referred as follows.

1. Choose the trial parameters of SDM column-reinforced soil, including d , D , B , l_1 , and l_2 . Then calculated the replacement ratio of SDM column, m , the core ratio, α . Based on the strength of DM column, estimate the coefficient of earth pressure and the interface friction angle of DM column and core pile, φ_i .
2. Use the parameters of φ_i , d and αm to calculate b and a .
3. Calculate E_I^{eq} , E_{II}^{eq} and p_c from Eqs. (7), (20) and (14b), respectively. For multiple soil layers, $E_{sl} = (E_{s1}l_{11} + E_{s2}l_{12} + \dots + E_{sn}l_{1n})/l_1$, in which E_{si} and l_{1i} is the constrained modulus and thickness of

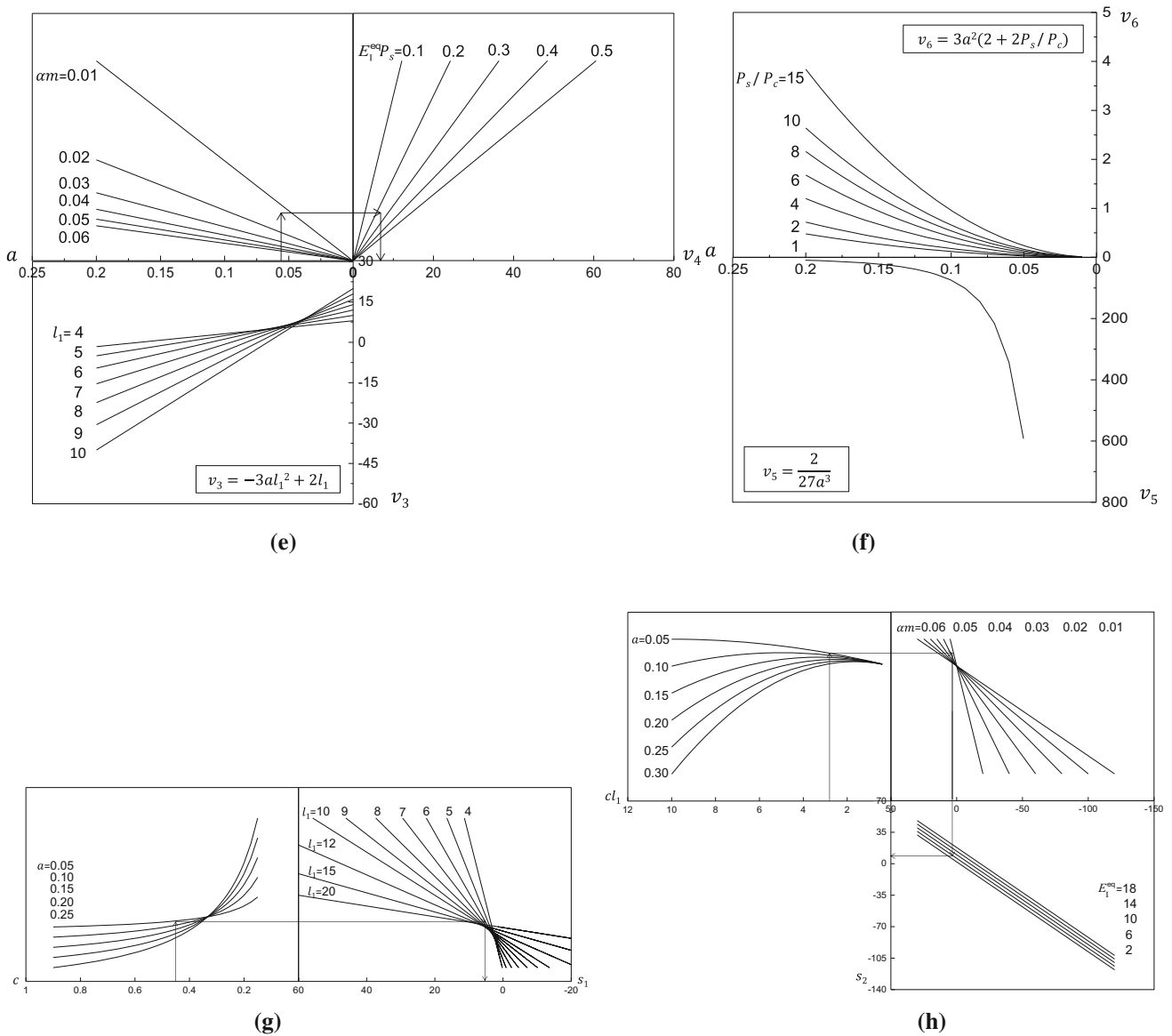


Fig. 12 continued

each layer in Region I. Determine p_s and p_s/p_c from the design chart (Fig. 12a).

4. Use Fig. 12b, c to obtain $u_1, u_2, u_3,$ and u_4 . Calculate $u = ((u_1 - u_2)/u_3 - u_4)/l_1^2$.
5. Use Fig. 12d–f to determine v_1 to v_6 . Calculate $v = ((v_1 + v_2)/(2 + 2p_s/p_c) + (v_3 - v_4)/v_6 - v_5)/l_1^3$
6. Based on step 5, use Table 7 to obtain the solution x , and $c = x + 1/(3al_1)$.
7. Use Fig. 12g, h to determine s_1 and s_2 , and then the settlement coefficient of region I can be calculated as $\psi = s_1/s_2$,
8. The settlement of Region I can be obtained by $S_I = P\psi$.

5 Application of the proposed method

5.1 Test embankment in AIT campus, Thailand [33]

Voottipruex et al. [33] conducted a large scale field test of SDM column-supported embankment at the northern part of the Asian Institute of Technology (AIT) Campus, Thailand. Figure 13 shows the configuration of the test embankment. Voottipruex et al. [33] introduced the geotechnical conditions and the test procedures on this site in detail. Therefore, this section only provides a brief summary. The test embankment consisting of a 1-m-thick sand cushion and 5-m-thick embankment fill was constructed with end slopes of 1:1 and side slopes of 1:1.5. The

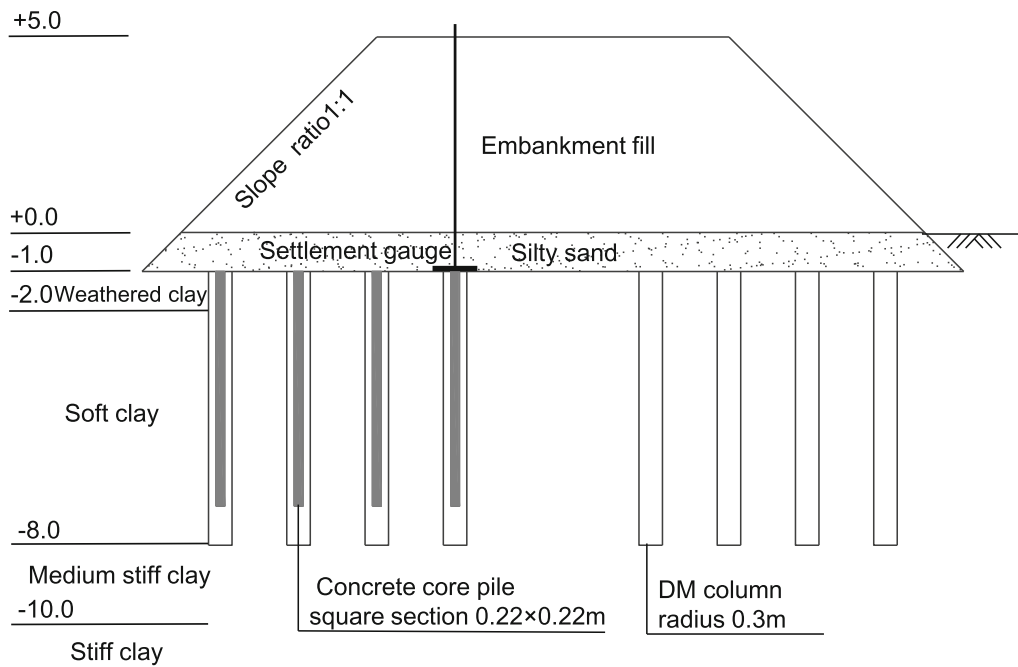


Fig. 13 Test embankment (unit: m, after Voottipruex et al. [33])

Table 3 Main properties of materials in the test

Materials	L (m)	E (MPa)	γ (kN/m ³)	μ	φ (°)	c (kPa)	k (m/d)
Embankment fill	5	30	16	0.30	20	10	1×10^{-3}
Silty sand cushion	1	30	17	0.30	25	0	1.0
Weathered crust	1	2.5	17	0.25	23	10	1×10^{-3}
Soft clay	6	2.5	15	0.25	23	2	4×10^{-4}
Medium stiff clay	2	5	18	0.25	25	10	2×10^{-4}
Stiff clay	15	9	19	0.25	26	30	4×10^{-4}

L , thickness; E , constrained modulus; γ , unit weight; μ , Poisson’s ratio; φ , friction angle; c , cohesion; k , coefficient of permeability

Table 4 Settlements by the proposed method and by the field monitor data (mm)

Method	Region I	Region II	Region III	Total settlement
Proposed method	42.4	13.1	108.4	163.9
Asaoka method	N/A	N/A	N/A	161.3

test embankment had base dimensions of 21 m × 21 m and top dimensions of 9 m × 6 m. The SDM columns with a diameter of 0.6 m and a length of 7 m were installed in a square pattern at a spacing of 2.0 m. The concrete core piles had a square cross section of 0.22 m × 0.22 m and a

length of 6 m. Table 3 shows the main properties of the soil layers and the SDM columns used in the field test, which were provided by Voottipruex et al. [33].

The side length of core pile $d = 0.22$ m, so $\alpha m = 0.0121$. Considering the core pile was directly pushed into the soil, a relative large K was selected herein (i.e., it is assumed to be the coefficient of passive lateral earth pressure in the design). The friction angles of DM column was taken as 30° [2, 13, 23, 43] and the interfacial friction angle between the DM column and the core pile was taken as 18° [31], and it can be calculated that $b = 5.8$, and $a = 0.055$.

The equivalent modulus of Region I is 5.0 MPa. The equivalent modulus of Region II is 5.5 MPa. The Poisson’s

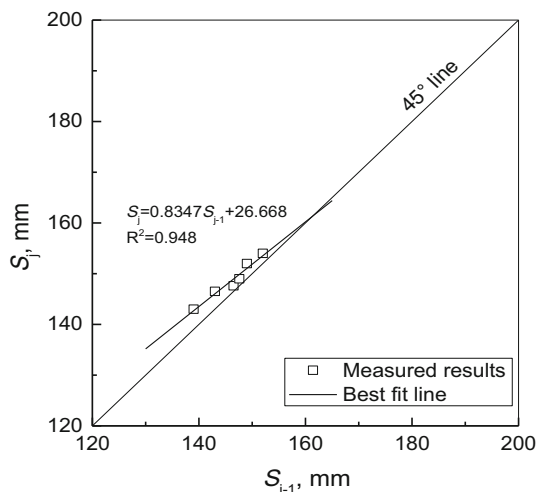


Fig. 14 Final settlement predicted by Asaoka method

ratio μ_0 is 0.33, $p_c = l_{SC}/E_c = 0.0333$, using $d = 0.22$ m, $E_{II}^{eq} = 5.5$ MPa, and it can be obtained from Fig. 12a that $p_s = 0.046$, $p_s/p_c = 1.38$.

The length of Region I (l_1) is 6 m, using $a, \alpha m, E_{II}^{eq}, p_s$, it can be obtained from Fig. 12b, c that $u_1 = 1, u_2 = 1, u_3 = 0.043, u_4 = 110.2$. So $u = ((u_1 - u_2)/u_3 - u_4)/l_1^2 = -3.06$. Similarly, it can be obtained from Fig. 12d–f that $v_1 = 216, v_2 = 400, v_3 = 6.1, v_4 = 6.6, v_5 = 445.2, v_6 = 0.043$. So $v = ((v_1 + v_2)/(2 + 2p_s/p_c) + (v_3 - v_4)/v_6 - v_5)/l_1^3 = -1.52$. It can be obtained from Table 4 that $x = -0.56, c = x + 1/(3al_1) = 0.45$.

Using c, a, l_1 , it can be obtained from Fig. 12g, h that $s_1 = 4.7, s_2 = 8.8$. So $\psi = s_1/s_2 = 0.53$, the maximum loading is 80 kPa, so the settlement of Region I is $S_I = P\psi = 80 \times 0.53 = 42.4$ mm.

According to Jones’s solution, the key parameters can be summarized as follows: ① $k_1 = E_1/E_2 = 5/5.5 = 0.91$, ② $k_2 = E_2/E_3 = 5.5/9 = 0.61$, ③ $H = h_1/h_2 = 6/3 = 2$, ④ $a_1 = r/h_2 = 11.85/3 = 3.95$.

Using linear interpolation, the vertical stress of Region II can be obtained as $\sigma_1 = 0.91 \times 80, \sigma_2 = 0.89 \times 80$, and the vertical stress on the bottom of medium stiff clay is 0.85×80 , so the settlement of Region II is $S_{II} = [(\sigma_1 + \sigma_2)l_2]/(2E_{II}^{eq}) = 13.1$ mm. The settlement of medium stiff clay is 25.3 mm.

The coefficient of average superimposed stress η in third layer is 0.7, so the settlement of Region III is $S_{III} = \eta\sigma_2 l_3/E_{III} + 25.3 = 108.4$ mm.

Figure 14 shows the variation of the ground settlement with time. According to the Asaoka method [3], the final settlement can be predicted based on the field data (see Fig. 11b), $s_\infty = 161.3$ mm. Table 4 presents the comparison of the settlement calculated using the proposed

method with that using Asaoka method and they agreed well with each other.

5.2 Field test in Nanjing, China [34]

Wang et al. [34] introduced two sections of field test of SDM column-supported embankment over soft soil at Nanjing Surrounding Expressway. Figure 15 shows the cross section of the two field tests. The SDM columns with a diameter of 0.5 mm were installed in a triangle pattern to a depth of 19.5 m. The column spacing was 1.5 m and 1.7 m in Site A and Site B, respectively. The width of embankment was 34.5 m with a side slope of 1:1.5. Table 5 shows the material properties in each test site.

Table 6 shows the final settlements predicted by the proposed method and the Asaoka method [3]. The good agreements were obtained. Based on the application in the two field tests, it can be concluded that the proposed method is feasible for calculation of the SDM column-supported embankment over soft soil.

6 Conclusion

Assuming the soil to be settled as one-dimensional deformation, this paper proposed an analytical method for calculating the settlement of SDM column-supported embankment over soft clay. The proposed method was verified by a comparison with the 3-D numerical model and field data. A parametric study was conducted to investigate the settlement characteristics of SDM column-supported embankment over soft soil. Based on the analysis and discussion, the following conclusions can be drawn.

- (a) Considering the upward and downward penetration effects of concrete core pile and the geometry characteristics in the cross section, the unit cell model was established, and the solution of the settlement of SDM column-reinforced soil was developed. The results by the developed solution agreed well with the results by the 3-D finite element models with three typical configurations.
- (b) The settlement of SDM-reinforced soft soil is reduced by increasing the modulus, diameter and length of DM column, the length of core pile. The cross section area of core pile and the interface friction angle had a minor influence on the settlement. From a practical point of view, increasing the length of core pile is the preferred option on mitigating the settlement of soft soil when adopting the SDM column, and the optimal length and diameter of core pile should be considered in design.

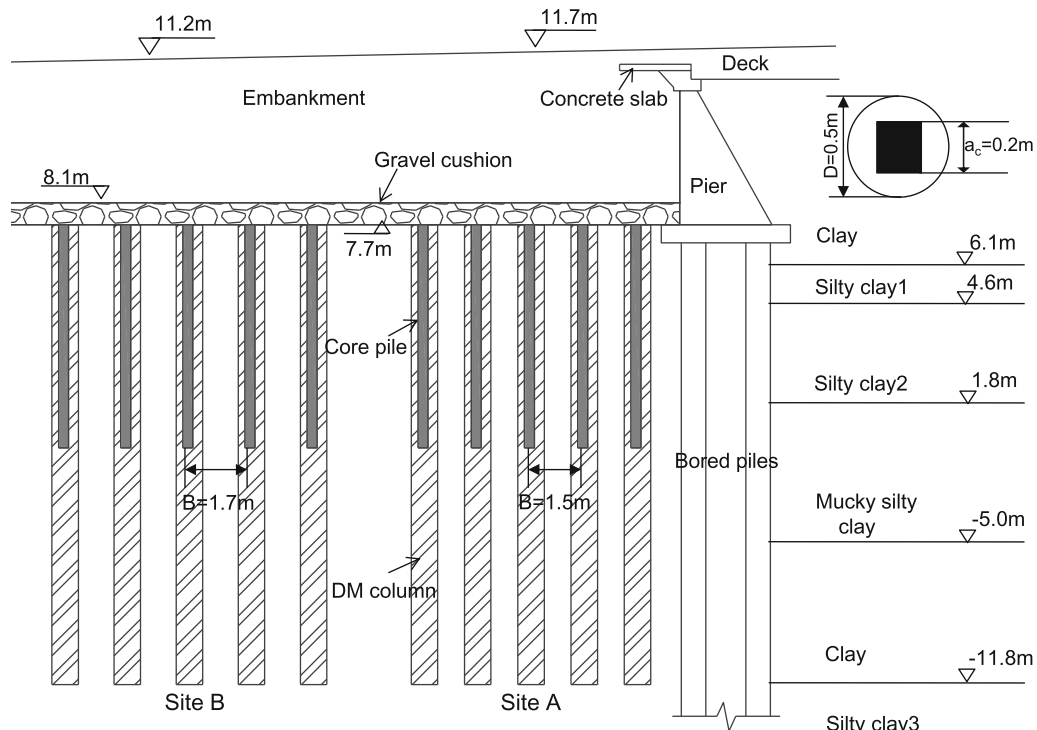


Fig. 15 Profile of SDM columns improved area (after Wang et al. [34])

Table 5 Main parameters of subsoils

Materials	L (m)	E (MPa)	γ (kN/m ³)	μ	φ (°)	c (kPa)
Clay	1.6	7.2	18.5	0.42	15.2	15.1
Silty clay 1	1.5	4.5	18.0	0.40	15.2	10.2
Silty clay 2	2.8	4.5	18.4	0.40	14.4	11.3
Mucky clay	6.8	2.5	18.3	0.44	17.0	9.5
Clay	6.8	4.5	19.0	0.42	16.5	11.7
Silty clay 3	15.0	13.5	19.1	0.40	22.0	22.3

Table 6 Comparison of proposed method with field data (mm)

Test site	Method	Region I	Region II	Region III	Total settlement
Site A	Proposed method	22.1	34.8	39.7	96.6
	Field data	N/A	N/A	N/A	100.8
	Asaoka method	N/A	N/A	N/A	107.3
Site B	Proposed method	27.5	40.9	40.9	109.3
	Field data	N/A	N/A	N/A	108.9
	Asaoka method	N/A	N/A	N/A	119.5

(c) The design procedure as well as design charts were developed for the calculation of settlement of SDM column-reinforced soft sol. The design method was applied to two case histories of SDM column-supported embankments and a good agreement was found between the predicted settlements and the field measurements.

Acknowledgements The authors appreciate the financial support provided by the Natural Science Foundation of China (NSFC) (Grant Nos. 51508408, 41772281) and by the Fundamental Research Funds for the Central Universities (Grant No. 22120180106) for this research.

Appendix

The contents in appendix are shown in Table 7 and Fig. 15.

Table 7 Solving univariate cubic equation

v	u															
	-0.05	-0.1	-0.5	-1.0	-2.0	-3.0	-4.0	-5.0	-6.0	-7.0	-8.0	-9.0	-10.0			
-0.0025	-0.053	-0.025	-0.005	-0.003	-0.001	-0.001	-0.001	-0.001	0	0	0	0	0			
-0.005		-0.051	-0.01	-0.005	-0.002	-0.001	-0.001	-0.001	-0.001	0	0	0	0			
-0.01		-0.115	-0.02	-0.01	-0.003	-0.003	-0.003	-0.002	-0.002	-0.001	-0.001	-0.001	-0.001			
-0.05			-0.102	-0.05	-0.017	-0.013	-0.013	-0.01	-0.008	-0.007	-0.006	-0.006	-0.005			
-0.1				-0.101	-0.033	-0.025	-0.025	-0.02	-0.017	-0.014	-0.013	-0.011	-0.01			
-0.5					-0.168	-0.125	-0.125	-0.1	-0.083	-0.071	-0.063	-0.056	-0.05			
-0.75					-0.256	-0.189	-0.189	-0.151	-0.125	-0.107	-0.094	-0.083	-0.075			
-1.0					-0.347	-0.254	-0.254	-0.202	-0.167	-0.143	-0.125	-0.111	-0.10			
-1.25					-0.446	-0.321	-0.321	-0.253	-0.21	-0.179	-0.157	-0.139	-0.125			
-1.5					-0.558	-0.39	-0.39	-0.306	-0.253	-0.216	-0.188	-0.167	-0.15			
-1.75					-0.695	-0.462	-0.462	-0.359	-0.296	-0.252	-0.22	-0.195	-0.176			
-2.0						-0.539	-0.539	-0.414	-0.34	-0.289	-0.252	-0.223	-0.201			
-2.25						-0.623	-0.623	-0.471	-0.384	-0.326	-0.284	-0.252	-0.226			
-2.5						-0.717	-0.717	-0.53	-0.43	-0.364	-0.316	-0.28	-0.252			
-3.0								-0.657	-0.524	-0.441	-0.382	-0.338	-0.303			
-3.5								-0.804	-0.624	-0.52	-0.449	-0.396	-0.354			
-4.0									-0.732	-0.603	-0.517	-0.455	-0.407			
-6.0										-1.0	-0.819	-0.706	-0.624			
-8.0											-1.236	-1.0	-0.865			

References

- Abdelkrim M, Buhan PD (2007) An elastoplastic homogenization procedure for predicting the settlement of a foundation on a soil reinforced by columns. *Eur J Mech A Solids* 26(4):736–757
- Ahnberg H, Johansson SE (2005) Increase in strength with time in soils stabilized with different types of binder in relation to the type and amount of reaction products. In: International conference on deep mixing best practice and recent advances, deep mixing, May 23–25, Stockholm, Sweden, pp 195–202
- Asaoka A (1978) Observation procedure for settlement prediction. *Soils Found* 18(4):87–101
- Bjerrum L, Johannessen IJ, Eide O (1969) Reduction of negative skin friction on steel piles to rock. In: Proceedings of the 7th international conference on soil mechanics and foundations engineering, Mexico, vol 2, pp 27–34
- Cao W, Chen Y, Wolfe W (2014) New load transfer hyperbolic model for pile–soil interface and negative skin friction on single piles embedded in soft soils. *Int J Geomech* 14(1):92–100
- Castro J, Sagaseta C (2011) Deformation and consolidation around encased stone columns. *Geotext Geomembr* 29(3):268–276
- Castro J (2014) An analytical solution for the settlement of stone columns beneath rigid footings. *Acta Geotech* 11(2):1–16
- Chai JC, Miura N, Kirekawa T, Hino T (2010) Settlement prediction for soft ground improved by columns. *Ground Improv* 163(G12):109–119
- Chen XF (2005) The theory and building cases of settlement computation, vol 2. Science Publication, Beijing, p 34 (in Chinese)
- Clemente FM Jr. (1984) Downdrag negative skin friction and hitumen coatings on prestress concrete piles. Ph.D. thesis, Tulane University, New Orleans
- Ding YJ, Li JJ, Liu E, Li H. Load transfer mechanism of reinforced mixing pile. *J Tianjin Univ* 43(6):530–536 (in Chinese)
- Elias V, Welsh J, Warren J, Lukas R, Collin JG, Berg RR (2006) Ground improvement methods, FHWA NHI-06-020. Federal Highway Administration, Washington
- Euro Soil Stab (2002) Development of design and construction methods to stabilise soft organic soils—design guide: soft soil stabilization, CT97-0351, Project No. BE 96-3177. IHS BRE Press, Watford
- Fukuya T, Todoroki T, Kasuga M (1982) Reduction of negative skin friction with steel tube NF pile. In: Proceeding of 7th Southeast Asian geotechnical conference, Hong Kong, vol 1, pp 333–347
- Han J, Oztoprak S, Parsons RL, Huang J (2007) Numerical analysis of foundation columns to support widening of embankments. *Comput Geotech* 34(6):435–448
- Han J, Wayne M H (2009) Settlement calculation of deep mixed foundations. In: Proceedings of international symposium on deep mixing and admixture stabilization, Okinawa, Japan
- Han J (2010) Consolidation settlement of stone column-reinforced foundations in soft soils. Invited, New technologies on soft soils. In: Almeida M (ed) Proceedings of symposium on new techniques for design and construction on soft clays, Brazil, pp 167–179
- Horikoshi K, Randolph MF (1999) Estimation of overall settlement of piled rafts. *Soils Found* 39(2):59–68
- Huang J, Han J (2009) 3-D coupled mechanical and hydraulic modeling of a geosynthetic-reinforced deep mixed column-supported embankment. *Geotext Geomembr* 27(4):272–280
- Jamsawang P, Bergado DT, Voottipruex P (2011) Field behaviour of stiffened deep cement mixing piles. *Proc Inst Civ Eng Ground Improv* 164(1):33–49
- Jeong S, Lee J, Lee CJ (2004) Slip effect at the pile-soil interface on dragload. *Comput Geotech* 31(2):115–126
- Jones A (1962) Tables of stressed in three-layer elastic systems. *Highw Res Board Bull* 342:176–214
- Kitazume M, Terashi M (2014) Deep mixing method. In: Dictionary geotechnical engineering/Wörterbuch GeoTechnik. Springer, Berlin
- Kong GQ (2009) Study on the characteristics of negative skin friction for pile groups. Ph.D. thesis, Dalian University of Technology, Dalian (in Chinese)
- Li N, Suleiman MT, Raich A (2016) Behavior and soil–structure interaction of pervious concrete ground-improvement piles under lateral loading. *J Geotech Geoenviron Eng* 142(2):04016045
- Liu SY, Du YJ, Yi YL, Puppala AJ (2015) Field investigations on performance of T-shaped deep mixed soil cement column-supported embankments over soft ground. *J Geotech Geoenviron Eng* 138(6):718–727
- Madun A, Jefferson I, Fook Y, Chapmand N, Culshawm G, Atkinps R (2012) Characterization and quality control of stone columns using surface wave testing. *Can Geotech J* 49(9):1357–1368
- Mankbadi R, Mansfield J, Ramakrishna A (2008) Performance of geogrid load transfer platform over vibro-concrete columns. In: Geocongress, pp 748–756
- Petchgate K, Jongpradist P, Panmanajareonphol S (2003) Field pile load test of soil–cement column in soft clay. In: Proceedings of the international symposium 2003 on soil/ground improvement and geosynthetics in waste containment and erosion control applications, Bangkok, Thailand, pp 175–184
- Raongiant W, Jing M (2013) Field testing of stiffened deep cement mixing piles under lateral cyclic loading. *Earthq Eng Eng Vib* 12(2):261–265
- Tanchaisawat T, Suriyavanagul P, Jamsawang P (2008) Stiffened deep cement mixing (SDCM) pile: laboratory investigation. In: International conference on concrete construction, London, 2008, pp 39–48
- Tinoco J, Correia AG, Cortez P (2011) Application of data mining techniques in the estimation of the uniaxial compressive strength of jet grouting columns over time. *Constr Build Mater* 25(3):1257–1262
- Voottipruex P, Bergado DT, Suksawat T, Jamsawang P (2011) Behavior and simulation of deep cement mixing (DCM) and stiffened deep cement mixing (SDCM) piles under full scale loading. *Soils Found* 51(2):307–320
- Wang Chi XuYF, Ping D (2014) Working characteristics of concrete-cored deep cement mixing piles under embankments. *J Zhejiang Univ Sci A (Appl Phys Eng)* 15(6):419–431
- White DJ, Pham HTV, Hoevelkamp KK (2007) Support mechanisms of rammed aggregate piers. I: experimental results. *J Geotech Geoenviron Eng* 133(12):1503–1511
- Wong KS, Teh CI (1995) Negative skin friction on piles in layered deposits. *J Geotech Eng* 121(6):457–465. [https://doi.org/10.1061/\(ASCE\)0733-9410\(1995\)121:6\(457\)](https://doi.org/10.1061/(ASCE)0733-9410(1995)121:6(457))
- Wu M, Dou YM, Wang EY (2004) A study on load transfer mechanism of stiffened DCM pile. *Chin J Geotech Eng* 26(3):432–434 (in Chinese)
- Yao K, Yao Z, Song X, Zhang X, Hu J, Pan X (2016) Settlement evaluation of soft ground reinforced by deep mixed columns. *Int J Pavement Res Technol* 9(6):460–465
- Ye GB, Zhang Z, Han J, Xing HF, Huang MS, Xiang PL (2013) Performance evaluation of an embankment on soft soil improved by deep mixed columns and prefabricated vertical drains. *ASCE J Perform Constr Facil* 27(5):614–623
- Ye GB, Cai YS, Zhang Z (2016) Numerical study on load transfer effect of stiffened deep mixed column-supported embankment over soft soil. *KSCE J Civ Eng* 21(3):1–12

41. Zhang L, Zhao M, Shi C, Zhao H (2013) Settlement calculation of composite foundation reinforced with stone columns. *Int J Geomech* 13(3):248–256
42. Zhang Z, Xing H, Ye G (2015) Consolidation analysis of soft soil improved with short deep mixed columns and long prefabricated vertical drains (PVDs). *Geosynth Int* 22(5):1–14
43. Zhang BJ, Huang B, Fu XD (2015) An experimental study of strength and deformation properties of cemented soil core sample and its constitutive relation. *Rock Soil Mech* 36(12):3417–3424
44. Zhao MH, Liu M, Zhang R, Long J (2014) Calculation of load sharing ratio and settlement of bidirectional reinforced composite foundation under embankment loads. *Chin J Geotech Eng* 36(12):2161–2169 (**in Chinese**)
45. Zheng G, Jiang Y, Han J, Liu YF (2011) Performance of cement-fly ash-gravel pile-supported high-speed railway embankments over soft marine clay. *Mar Georesour Geotechnol* 29(2):145–161

Publisher's Note Springer Nature remains neutral with regard to jurisdictional claims in published maps and institutional affiliations.